Heliyon 10 (2024) e30399

Contents lists available at ScienceDirect

Heliyon

journal homepage: www.cell.com/heliyon

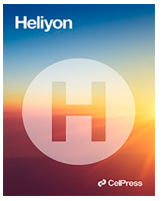

Research article

Understanding the drying mechanism of straw substrate culture block: Physicochemical properties, pore structure, and drying optimization

Qian Cheng, Zihui Liu, Jiayi Sun, Shuo Li, Chongxuan Zhao, Junfeng Su, Qingyu Liu, Mingjin Xin, Dejun Liu *

College of Engineering, Shenyang Agricultural University, Shenyang, 110866, China

ARTICLE INFO

Keywords:
Substrate culture block
Drying mechanism
Pore structure
Pore modeling
Moisture migration

ABSTRACT

As a new type of agricultural waste block substrate utilization, the initial wet base state of the substrate culture block needs to be dried. Therefore, studying the drying mechanism of substrate culture block is critical. In this study, the substrate culture block in a dry state was taken as the research object. Based on physical and chemical properties, the internal section of the substrate culture block was characterized by scanning electron microscopy and the pore condition of the particles was quantified. The results showed that the internal pore structure was uniform and favorable for plant root growth. Based on the pore structure, pore channel modeling was constructed to investigate the distribution of the internal multiphase medium and to distinguish between channels and pore-blind channels. The applicability of the modeling was verified and discussed. By measuring the drying rate of the substrate culture block and classifying its drying stages as fast speed, constant speed, and slow speed, it is clarified that the forms of moisture existence are bound-state water and free-state water, and the moisture migration is prioritized as surface adsorption water, interparticle water, particle attached water, and capillary water. Innovate a method to quantify the change of pore space in the drying process by pore coefficient ratio to evaluate the drying quality. The results show that when the pore coefficient ratio is about 40 %, its moisture content is 20 %~30 %, and the drying effect is best at this time. The physical drying test further confirmed the correctness of the conclusion of the drying stage division and water loss law. This study can provide a theoretical reference for the modeling study of the pore structure of the block matrix and the exploration of its drying mechanism.

1. Introduction

Half of the photosynthesis products in crops are allocated to seeds, while the other half is present in straw, which refers to the fibrous plant residue remaining after seed harvest. As a renewable biomass resource, Straw holds significant quantities and serves various purposes [1]. The issue of straw utilization has garnered public attention in recent years, as its proper usage is closely linked to environmental factors such as air quality, global nitrogen and carbon cycles, agricultural productivity, and sustainable development [2]. The comprehensive utilization of straw encompasses several aspects, including fertilizer utilization [3,4], fuel utilization [5,6],

* Corresponding author.
E-mail address: ldjldj@syau.edu.cn (D. Liu).

https://doi.org/10.1016/j.heliyon.2024.e30399
Received 24 November 2023; Received in revised form 24 April 2024; Accepted 25 April 2024
Available online 30 April 2024

substrate utilization [7,8], feed utilization [9,10], and raw material utilization [11–13]. Among these applications, straw substrate utilization is widely employed in agriculture due to its advantageous features, including ease of production, cost-effectiveness, adjustable nutrient levels, and minimal environmental impact. Straw substrate utilization involves the processing or preparation of organic solid materials, primarily straw as the primary raw material, to create favorable conditions and specific nutrients for the growth of animals, plants, and microorganisms.

In recent years, agro-waste substrates such as earthworm manure substrate [14], cocopeat compound substrate [15], and biochar substrate [16] have gained significant traction in the realm of soilless cultivation and urban agriculture. Their usage in various urban applications, including balcony agriculture [17], green roofs [18], and green gardens [19] are gradually becoming more recognized. Consequently, the demand for soilless substrates as growing mediums has surged. However, certain limitations regarding nutrient provision, pore condition, water retention capacity, and storage and mobility properties impede the widespread adoption of straw-based substrates. Therefore, addressing these constraints is crucial to promote the popularization of straw-based substrates. The adjustability and ability to supplement nutrients make substrates suitable for providing necessary nutrients during plant cultivation and subsequent stages of plant culture. Adding perlite can enhance the regulation of pore space within the substrate. While constant watering at a later stage can meet the water requirements for plant growth, it inevitably increases maintenance time and costs. Substrates' storage and mobility in bulk form could be more convenient. Recent research has focused on utilizing agricultural waste as solid block substrates in cultivation. These applications include substrate nursery blocks [20], seedling block bricks [21], greening substrate bricks [22], and substrate grass seed blankets [23]. These applications primarily utilize crop residues like rice straw and corn stover as substrate materials. Other components, such as cow dung, are added and physically compressed and molded to form solid block substrates for growing mediums and seedling breeding purposes [24–27].

The substrate culture block, with natural plant fibers and organic fertilizers as the basic raw materials, is fixed by the mold under a certain pressure to make the degraded crude fat, crude protein, intestinal secretion, and shedding cuticle thoroughly intertwined, entangled, and integrated, and then formed into the substrate culture block. The substrate culture block is highly versatile in shape and can be easily molded to meet the diverse requirements of plant growth. Depending on the needs, crops can be planted directly onto the substrate culture block, or seeds can be added during the molding stage and subsequently dried, stored, or transported. The blocks have excellent storage and transportation properties, making them suitable for long-distance transportation, palletization, and flat paving. Furthermore, the substrate culture block is adaptable to various cultivation environments, and after watering, it retains its original shape while providing essential nutrients to the plants. The block's loose and porous structure facilitates integration with the original ground surface, rapidly establishing a substrate layer. The process eliminates the isolation layer between the substrate and soil layers, promoting water retention nutrient conservation, and enhancing the overall soil quality. The substrate culture block finds extensive applications in different scenarios, including factory nurseries and ecological restoration projects such as soil improvement, sand greening, and slope greening. It provides a long-term, high-quality growing environment for plants, gradually improving soil conditions while supporting sustainable agriculture practices.

Developing growing medium blocks resolves the complex challenges of collecting, storing, and transporting urban soil, offering significant application prospects and a broad market for substrate culture blocks. However, during transportation, the wet state of the substrate culture block can lead to situations where it becomes loose or breaks apart. In order to avoid such situations, the substrate culture blocks undergo a drying treatment to achieve a specific anti-destructive strength and a proven solution after drying. The dried substrate culture block needs to possess several characteristics. It should have a lightweight texture, making it resistant to loosening and breaking under external forces. Additionally, it should exhibit anti-destructive capabilities and be easy to pack and transport, thus reducing transportation costs. Furthermore, the performance of the dried substrate culture block must remain consistent when subjected to water moistening treatment, maintaining its shape and meeting the water, nutrient, and trace element requirements of growing crops. Achieving these objectives requires a comprehensive and controlled drying process, which necessitates in-depth research on the microstructure and drying characteristics of the growing medium block.

The substrate culture block falls under the category of porous medium materials, which are characterized by a significant internal surface area due to the presence of pores, voids, or cracks [28–30]. The abundant pore structure offers attachment sites for water, facilitating water retention within the substrate. Water transport occurs in the pores and the matrix during the drying process. Therefore, comprehensively exploring the microscopic pore structure of the substrate culture block is paramount. Understanding the drying law and characteristics of the substrate culture block provides a valuable reference for the drying of large quantities of these blocks, aiding in their commercialization.

Fig. 1. Substrate culture block object. (a) Material form of the substrate culture block, (b) Form of the substrate culture block, (c) Cultivation form of the substrate culture block.

2. Materials and methods

2.1. Test materials

The composition of the substrate culture block is illustrated in Fig. 1(a). In this study, rice straw fiber was chosen as the natural plant fiber, which was obtained from a farmer's field in Shilihe Town, Sujiatun District, Shenyang City, in October 2020. The specific variety used was Northern Japonica 1705. Organic fertilizers were sourced from Liaoning Huishan Dairy Group in Shenbei New District, Shenyang City, and consisted of rotted cow dung. The rice straw was collected after harvest, naturally dried in the field, and then crushed. Subsequently, it was sieved through a 10 × 10 mm mesh sieve. The ripened cow dung was mixed with the sieved rice straw at a ratio of 3:1. This mixture underwent a maturation process and was compacted in a specific mold to produce substrate culture blocks in the form of bricks measuring 300 × 200 × 60 mm as depicted in Fig. 1(b). The initial water content of the blocks in a wet state was approximately 80 %, with a total mass of approximately 5000 g. The desired water content of the substrate culture blocks in a dry state was maintained at around 20 %. They were moistened with water to restore the blocks to a wet state suitable for plant cultivation. An illustration of an example of the substrate culture block is presented in Fig. 1(c). For this research paper, investigations and experiments will be conducted on the brick form of the substrate culture block depicted in Fig. 1(b).

2.2. Test methods

2.2.1. Determination of physical and chemical properties

The substrate culture block raw material is the bulk material form of the substrate culture block. The physical and chemical properties of the substrate culture block raw material were determined, and the physical properties of the raw material included bulk density, total porosity, aeration porosity, and water-holding porosity. The chemical properties included EC, pH, organic matter, TN, TP, TK, total organic carbon, cellulose, hemicellulose, lignin, and metal ion content. The measured physicochemical properties of the substrate culture block need to be compared with the standards of the Chinese national industry "LY/T 1970–2011 Organic media for greening use", "LY/T 2700-2016 Growing medium for flowering trees and shrubs" and "NY/T 2118-2012 Vegetable plug seedling substrate". The national industry standards are equivalent to international standards. The national industry standard has more specific requirements for substrates.

In order to analyze the physical properties of the substrate culture blocks, the raw materials were pressed to form the substrate culture blocks by using a substrate culture block pressing and forming tester. The bulk density and pore size were determined by the national environmental protection standard of the People's Republic of China and the agricultural industry standard "NY/T 2118-2012 Vegetable plug seedling substrate" and "HJ 613–2011 Soil-Determination of dry matter and water content-Gravimetric method". The substrate culture block was dried in an electric blast drying oven (Model: JKS-10, manufacturer: Beijing Yong Guangming Medical Instrument Co., Ltd., Beijing, China), and the volume of the substrate culture block was determined as V with a ruler, and the weight of the substrate culture block was determined as W_0 with a high-precision electronic scale (Model: YH-13, manufacturer: Shanghai Yingheng Weighing Equipment Co., Ltd., Shanghai, China). Saturated with water and weighing the mass no longer change recorded as W_1, the substrate culture block free to drain until no water oozing out and weighing the mass of W_2, according to the following Equations (1)–(4) to calculate the measurements:

$$BD = W_0 / V \tag{1}$$

$$TP = (W_1 - W_0) / V \times 100\% \tag{2}$$

$$AP = (W_1 - W_2) / V \times 100\% \tag{3}$$

$$WHP = TP - AP \tag{4}$$

where: V is the volume of the substrate culture block in cm^3; BD is the bulk density in g/cm^3; TP is the total porosity in %; AP is the aeration porosity in %; WHP is the water-holding porosity in %; W_0 is the mass of the substrate culture block in g; W_1 is the mass of the saturated submerged substrate culture block in g; and W_2 is the mass of the free-drained substrate culture block in g.

In order to analyze the chemical properties of the growing medium culture block, some of the raw materials were dried in an electric blast drying oven (Model: 101ES, manufacturer: Beijing Yong Ever Bright Medical Treatment Instrument Co., Ltd., Beijing, China), and then passed through a 5-mesh automatic standard vibration sieve (Model: A3-VS200, manufacturer: Shaoxing Dongjing Machinery Equipment Co., Ltd, Zhejiang, China). The samples were sieved until the particle size was less than 4 mm. Then, the samples were weighed to 10 samples of 100 g each and entrusted to the Qingdao branch of Shanghai Microspectrum Chemical Technology Co., Ltd. Referring to the national environmental protection standards of the People's Republic of China and agricultural industry standards "HJ 802–2016 Soil quality-Determination of conductivity-Electrode method", "NY/T 1121.2–2006 Soil Testing Part2: Method for determination of soil pH", "HJ 761–2015 Soil quality-Determination of organic matter-Ignition loss method", "NY/T 1121.16–2006 Soil Testing Part 16: Method for determination of total water-soluble salt".

The EC of the substrate culture block raw materials was determined by a conductivity meter (Model: S210–B, manufacturer: Shanghai Haokuo Scientific Equipment Co., Ltd., Shanghai, China) using the electrode method. The pH value was determined using a pH meter (Model: PH610, manufacturer: Julabo Technology (Beijing) Co., Ltd, Beijing, China). The organic matter content of the

substrate culture block was determined using a muffle furnace (Model: MFLXD111-12, manufacturer: Shanghai Muffle Furnace Technology Instrument Co., Ltd, shanghai, China). Determination of nitrogen, phosphorus and potassium in the substrate culture block was carried out according to the manual of the fully automatic chemical analyzer, and the main instruments used for the determination were the fully automatic chemical analyzer (Model: SmartChem200, manufacturer: Ams France, Paris, France) and the digestion instrument, intelligent microwave extractor (Model: XT-9900A, manufacturer: Shanghai XTrust Analytical Instrument Technology Co. Ltd., Shanghai, China). TOC was determined using a TOC analyzer (TOC-3000, manufacturer: Shanghai Yuanxi Analytical Instrument Co., Ltd., Shanghai, China). Cellulose, hemicellulose and lignin were determined using a fully automatic cellulose analyzer (Model: F2000, manufacturer: Hanon Advanced Technology Group Co., Ltd, Jinan, China). Metal ion content was determined using an inductively coupled plasma emission spectrometer (Model: Avio500, manufacturer: PerkinElmer Corporate Management (Shanghai) Co., Ltd, Shanghai, China).

2.2.2. Observation of internal structure surface characteristics

In order to investigate the internal microscopic characterization structure of the substrate culture block material, the substrate culture block was subjected to a scanning electron microscope (Model: Regulus 8100, manufacturer: Hitachi (China) Co., Ltd., Beijing, China), and the transverse section, radial section, and oblique section of the substrate culture block were observed. Comparative observation of the SEM images of the transverse section, radial section, and oblique section of the substrate culture block provides a comprehensive and adequate understanding of its internal microstructure [31]. The transverse section of the substrate culture block shown in Fig. 2(a) is perpendicular to the longitudinal axis where the growing medium plant is located; the radial section shown in Fig. 2(b) is perpendicular to the transverse section by passing through the center in the direction of plant growth; and the oblique section shown in Fig. 2(c) does not pass through the center and is at an angle to the transverse section. The images were processed with pseudo-colors using Image J software to improve the layering of the images, thus highlighting the microstructure [32]. The specific operation process is as follows: import the scanning electron microscope image into Image J software and select the coloring method of "blue orange icb" under the "lut" tab to complete the pseudo-color processing.

2.2.3. Pore and particle identification

Using the "stacks" option under the "image" option in the Image J software, we merged the substrate culture block transverse sections, radial sections, and oblique sections into an image stack. Then, we made a rectangular box for the SEM area. At this time, the rectangular box of the three sections had the same area. We used the "plot profile" tool in the "analyze" option to generate a line plot of the distance versus the grayscale value, which was used to represent the grayscale change in the rectangular box—the grayscale changes in the range through which the box is selected. The magnitude of the grayscale change per unit distance indicates pore size, and the continuity of the magnitude of the grayscale change indicates the pore coverage pattern [33]。

Scale correction was performed using "spatial calibration" under the "measure" option in the Image-Pro Plus software, and pore labeling was performed by selecting the "measurements" tool under the "measure" option, taking any three cross-sectional images and randomly labeling a total of 20 pores in each image for a total of 60 pores, and counting the pore aperture size distribution. Use "count/size" under the "measure" option for grayscale identification. Select ranges to get the pore labeling image and calculate the image porosity.

The SEM images of three cross-sections of the substrate culture block were identified and quantitatively analyzed using the particle (pores) and cracks analysis system (PCAS) software. The specific operation of the particles and pore space parameters obtained by PCAS software is as follows: After opening the image, the software selects "use rgb segmentation" and clicks on "segment" to obtain a binarized image. Set the "element radius" and the "minimum area". Click "auto analysis (region)" to automatically complete the pore identification, and click "statistic parameters" to get the statistical parameters of the pore [34]. Since the substrate culture particles are viscous, the closure radius is set to 2.1, and the minimum area of pores is set to 50 [35].

2.2.4. Pore channel modeling

The pore channel model of the substrate culture block was constructed based on the table structure and the structural characteristics of the porous medium [29]. Using a super depth-of-field 3D microscope (Model: VHX-5000, manufacturer: Keens (China) Co., Ltd., Shanghai, China) to scan a certain level of the substrate culture block to obtain the actual initial image Fig. 3(a), the image binarized by Matlab software to obtain the black-and-white image Fig. 3(b) [36], any partial Fig. 3(c) to zoom in Fig. 3(d), the simplification principle is to reduce the connection points to make the curve smooth, to obtain the orifice image Fig. 3(e) [37]. Fig. 3 shows the pore channel establishment process of the substrate culture block. Since the material structure of the substrate culture block is a porous medium, the material arrangement structure of different volumetric elements is considered to be the same, and thus, the

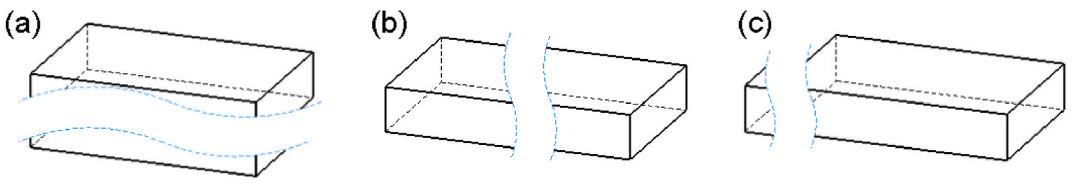

Fig. 2. Schematic diagram of each section of the substrate culture block. (a) Transverse section, (b) Radial section, (c) Oblique section.

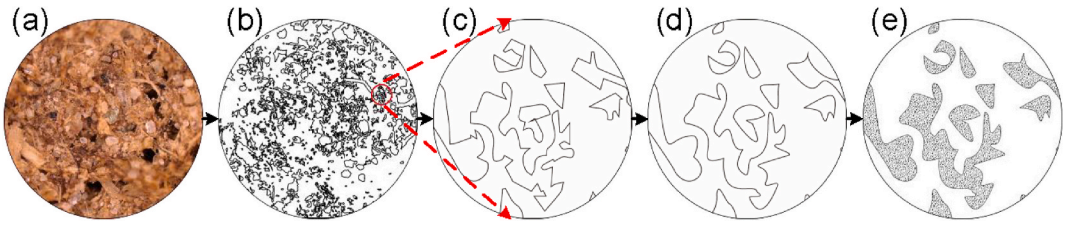

Fig. 3. The process of modeling the pore channel of substrate culture block. (a) Original image, (b) Binarized image, (c) Localized image, (d) Simplified image, (e) Pore channel image.

pore channel model established in this study can represent any volumetric element structure [38–40]. The pore channel modeling of the substrate culture block is well adapted since the modeling is shifted from a physical object in the construction process.

2.2.5. Material drying rate determination

The drying rate is the mass of moisture removed per unit of time, and the drying rate calculation formula is shown in Equation (5):

$$U = dW/Adt - G_C dX/Adt \tag{5}$$

where: U is the drying rate, also known as drying flux, unit kg/(m^2s); A is the drying surface area, unit m^2; W is the wet fraction of vaporization, unit kg; t is the drying time, unit s; G_C is the mass of the adiabatic material, unit kg; X is the wet content of the material, unit %.

The wet base state of the substrate culture block material was placed in a constant airflow for the drying test. With the increase of drying time and moisture vaporization, the wet base state of the material mass continues to decrease every 1 h to record the material mass G until the material mass is unchanged, that is, the material in the conditions of the drying limit until, at this time to stay in the material of the moisture is the equilibrium moisture X. Calculate the instantaneous moisture content X at each moment, and then X on the drying time t figure, that is, the drying curve. The formula for calculating the instantaneous moisture content X in the material is shown in Equation (6):

$$X = (G - G_C) / G_C \tag{6}$$

where: G_C is the mass of dehydrated material, unit kg; X is the wet content of the material, unit %.

2.2.6. Definition and determination of pore coefficient ratio

The prepared single-block substrate culture block was dried naturally because the pore changes were not evident briefly during the drying process. The pore changes were recorded every 15 h. The sample morphology of different drying stages was recorded. In contrast, the pore channel model was constructed, and pore coefficient ratios were calculated for different stages of the substrate culture block. The results of the calculations were averaged over three times. The pore changes during the drying process were analyzed to verify the correctness of the pore coefficient ratio to quantitatively analyze the changes of pore channels during the drying process.

Sections of substrate culture block samples with different drying times were processed. Pore images were scanned and extracted with a VHX-5000 super depth-of-field scanning microscope to analyze the characteristics of pore coefficients per unit area of substrate culture blocks with different drying degrees and to quantitatively analyze the changes of pore channels in the drying process. The pore coefficient ratios defined by combining with pore models are shown in Equation (7):

$$P = S_P/S_T \times 100\% \tag{7}$$

where: P is the pore coefficient ratio of the dry specimen, unit %; S_P is the area of the pore part of the dry specimen, unit mm^2; S_T is the total area of the image of the dry specimen, unit mm^2.

A single substrate culture block was prepared for the natural drying process. Due to the drying process within a short period, pore changes are not noticeable every 10 h to record the different drying stages of substrate culture block sample morphology, while the different stages of substrate culture block sampling pore channel modeling and pore coefficient ratio, the results of the calculation of the average value of the three times. The changes in pore space during the drying process were analyzed to verify the reasonableness and correctness of the pore coefficient ratio used to quantitatively analyze the changes in pore channels during the drying process.

2.2.7. Drying test monitoring arrangement

In order to verify the water size and water transport law at different points during the drying process of the substrate culture block, the prepared substrate culture block was put into an electric blast drying oven (Model: 101ES, manufacturer: Beijing Yong Guangming Medical Instrument Co., Ltd., Beijing, China) for the drying test and the temperature and humidity statistics were made for each point. Five points (A、B、C、D、E) were taken in the same plane of the substrate culture block for temperature and humidity measurements, and the probe of the temperature and humidity recorder (Model: Elitech-RC-4HA, manufacturer: Jiangsu Jingchuang Electrical Appliances Co. Ltd, Xuzhou, China) was inserted into the substrate culture block at a depth of 40 mm. The externally connected probe-

type temperature and humidity logger, the host and the probe are separated, equipped with an external temperature and humidity probe, 1 m extension lead, just put the probe into the environment to be measured to obtain data. Fig. 4(a) shows the layout of the monitoring points of the substrate culture block. Point A is the monitoring point at the center of the substrate culture block. Points D and E are the monitoring points at the edges in the diagonal direction. Points B and C are the monitoring points at the center in the other diagonal direction. The horizontal distance DA = EA = 2BA = 2CA, then the arrangement of the monitoring points can represent the overall situation of the substrate culture block and ensure the uniformity of its monitoring points.

According to the information, the electric heating blast drying box has an internal space size of 450 × 350 × 450 mm. The air supply mode is a side-end air supply with top-end air return, and the air velocity is 0.6 m/s. During the drying test, the substrate culture block was placed 100 mm away from the bottom of the compartment, a breathable hole board. The upper surface of the substrate culture block was 200 mm away from the upper side of the box. Fig. 4(b) demonstrates the arrangement of the drying test environment for the substrate culture block.

3. Results and analysis

3.1. Analysis of physical and chemical properties

After testing, the physical properties of the substrate culture block are shown in Table 1.

The findings indicate that the substrate culture block samples exhibited a measured bulk density of 0.62 g/cm^3. The total porosity was determined to be 68.52 %, consisting of an aeration porosity of 22.44 % and a water-holding porosity of 46.08 %. These physical property indicators, including bulk density and porosity, are well within the acceptable range for promoting plant growth. This confirms that the substrate culture blocks possess a compact structure with unchanged and stable properties while offering adequate permeability and water absorption. Consequently, they meet the physical requirements set forth by relevant Chinese standards, including those for organic media in greening applications, growing medium for flowering trees and shrubs, and vegetable seedling substrates.

The chemical properties of the substrate culture blocks are shown in Table 2.

The chemical properties of the substrate culture block align with the optimal range for supporting crop growth and effectively meet the standards outlined for organic media used in greening applications, growing mediums for flowering trees and shrubs, and vegetable seedling substrates. These properties adhere to the prescribed chemical requirements set for substrates in these standards.

3.2. Characterization of the internal microstructure

Scanning electron microscopy images (Figs. 5–7) revealed distinctive section shapes of the substrate culture block, including plate-like, ribbon-like, and pellet-like structures. The materials exhibited interlocking and integration, with some regions demonstrating adhesion. Irregularities in particle shape and arrangement contributed to the formation of voids between the material particles, ultimately connecting to create pores. These pores serve as spaces that can be filled with both air and water. During moistening, water fills the pore space while also permeating the material—consequently, the interconnected pore spaces form channels to facilitate the movement of fluids.

The transverse section of the substrate culture block was examined using scanning electron microscopy (SEM), as shown in Fig. 5 (a–c). It revealed a distinctive interlocked superposition-like structure, primarily resulting from the longitudinal compression force experienced during the molding stage. This compression led to pronounced flattening in this section, while the rice straw fibers exhibited intricate intertwining and formed a mesh-like pattern. Notably, the pore sizes within this section needed to be more balanced. Furthermore, the vertical transverse section displayed a deepening along the longitudinal direction. Consequently, longitudinal pores were present, providing ample space for the root system of cultivated plants to grow. The interlaced pore structure within the substrate block created a favorable environment for plant cultivation, mainly due to the interlocking spaces facilitating the development of the plant's root system. In the vertical direction of the plant root system, due to the interwoven and superimposed pore structure, the root growth encounters obstacles to extend in other directions, which leads to the interweaving of the plant root system into a mesh. The substrate provides nutrients to the plant as it is surrounded by the web of plant roots, resulting in more vigorous

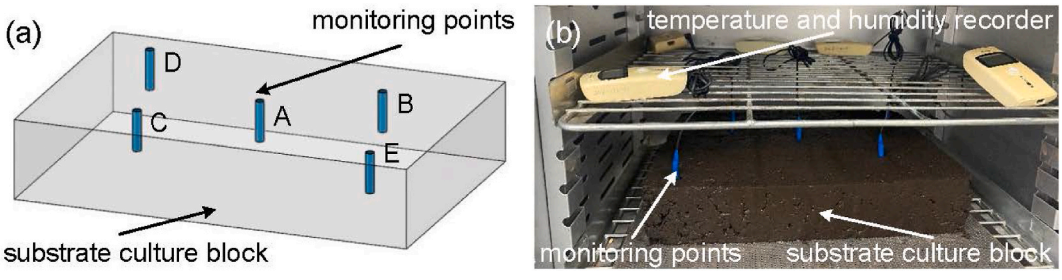

Fig. 4. Drying test condition arrangement of substrate culture block. (a) Schematic diagram of monitoring point arrangement, (b) Drying test environment arrangement.

Table 1
Physical properties of substrate culture block.

Physical properties	Test 1	Test 2	Test 3	Average value	LY/T 1970–2011	LY/T 2700-2016	NY/T 2118-2012
Bulk density, g/cm^3	0.60	0.57	0.63	0.62	0.10~0.80	0.30~1.80	0.20~0.60
Total porosity, %	68.45	67.94	69.17	68.52	–	50.00–90.00	>60.00
Aeration porosity, %	23.32	22.37	21.63	22.44	≥20.00	–	>15.00
Water-holding porosity, %	45.13	45.57	47.54	46.08	>45.00	–	>45.00

Note: Data statistics results rounded to two decimal places. “-" means that the indicator is not explicitly required under this standard.

Table 2
Chemical characterization of substrate culture block.

Chemical properties	Test 1	Test 2	Test 3	Average value	LY/T 1970–2011	LY/T 2700-2016	NY/T 2118-2012
EC, Ms/cm	0.53	0.59	0.56	0.56	0.35~1.50	0.10~2.00	0.10~0.20
Ph	5.76	6.01	5.84	5.87	5.00~8.00	5.00~8.50	5.50~7.50
Organic matter, %	35.56	36.64	38.14	36.78	≥20.00	–	≥35.00
TN, mg/kg	124.36	131.21	124.14	126.57	–	–	50.00~500.00
TP, mg/kg	12.34	13.89	14.12	13.45	–	–	10.00~100.00
TK, mg/kg	204.37	205.28	208.77	206.14	–	–	50.00~600.00
TOC, mg/g	161.12	164.43	160.81	162.12	–	–	–
Cellulose, %	25.43	28.31	26.60	26.78	–	–	–
Hemicellulose, %	22.98	23.47	27.56	24.67	–	–	–
Lignin, %	35.93	35.75	38.81	36.83	–	–	–
Ca, mg/kg	27.23	29.45	29.57	28.75	–	–	50.00~200.00
Cu, mg/kg	127.56	130.27	132.59	130.14	≤150.00	–	–
Fe, mg/kg	29.17	28.96	32.56	30.23	–	–	–
Mg, mg/kg	47.73	50.32	47.51	48.52	–	–	25.00~100.00
Mn, mg/kg	0.98	1.12	0.96	1.02	–	–	–
Na, mg/kg	6.13	6.25	6.34	6.24	–	–	–
Zn, mg/kg	285.57	286.71	284.01	285.43	≤300.00	–	–

Note: Data statistics results rounded to two decimal places. “-" means that the indicator is not explicitly required under this standard.

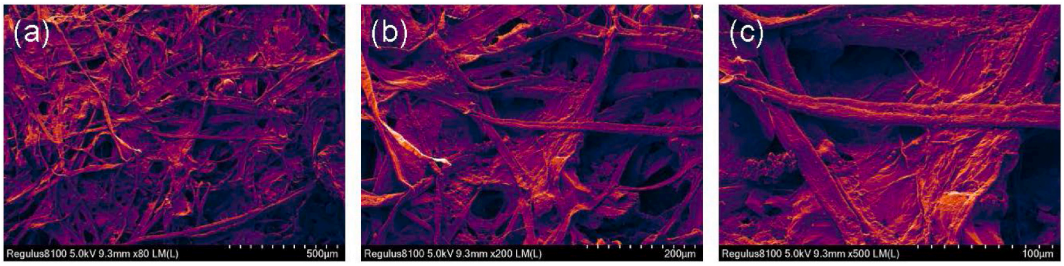

Fig. 5. Scanning electron micrographs of transverse sections of substrate culture blocks. (a) 80X, (b)200X, (c) 500X.

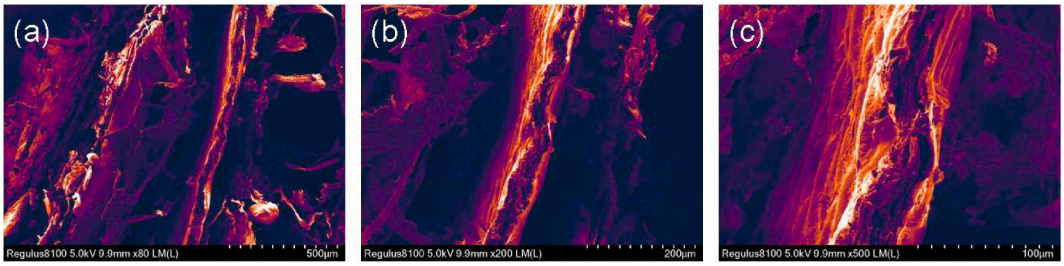

Fig. 6. Scanning electron micrographs of radial sections of substrate culture blocks. (a) 80X, (b) 200X, (c) 500X.

rooting of the cultivated plant.

During the molding stage, the growing medium culture block experiences longitudinal pressure, leading to delamination within its structure. This phenomenon is evident in the longitudinal section, as depicted in Fig. 6(a–c), where the continuous material is severed, resulting in visible faults. The pore structure is broken horizontally, which can provide space for the plant root system to grow. The

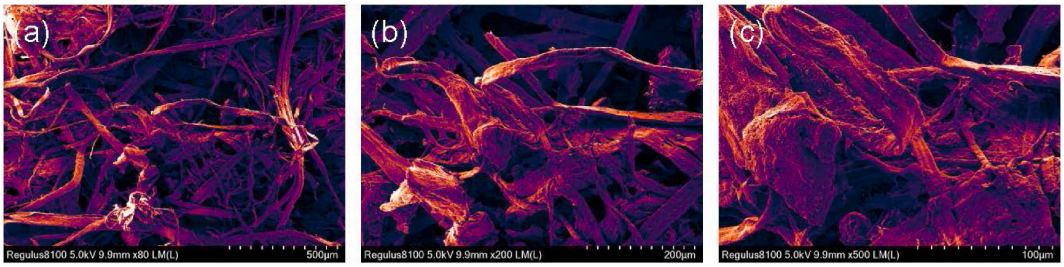

Fig. 7. Scanning electron micrographs of oblique sections of substrate culture blocks. (a) 80X, (b) 200X, (c) 500X.

plant root system's horizontal extension and vertical growth create a spatial enclosure where the root system can carry more substrate. The layered and faulted structure of the substrate culture block contributes to its advantageous water-holding and locking properties. As a result, it can effectively retain water and nutrients, ensuring a continuous supply for plants during cultivation.

The oblique section is shown in Fig. 7(a–c). Since the oblique section involves both transverse and longitudinal directions, the Table has a dispersed characterization shape, highlighting more ribbon-shaped rice straw fibers with cow dung particles interspersed in them, and the transverse and longitudinal pores are distinguishable. The pore structure in the oblique section is more three-dimensional and more reflective of actual conditions. Plant roots grow in all directions under this structure. The fully grown root system is intermingled with the pore structure.

Analysis of the three sections of the substrate culture block using SEM revealed abundant pore structures and pore spaces within the material. These internal features provide ample sites for water retention and facilitate water transportation through pore channels during the drying process. The rich pore structure stores more nutrients and water, providing a continuous supply of nutrients during the actual cultivation of the plant. Plants can continue to grow and develop even in complex external environments.

3.3. Quantitative analysis of pores and particles

Fig. 8 illustrates the variation in gray values across the three sections of the substrate culture block. The consistent fluctuation of the gray values indicates the presence of abundant pore structures within all three cross-sections. Moreover, the similarity in pore conditions among the three sections suggests that the substrate culture block can be considered a medium with uniformly distributed pore sizes in all directions.

Fig. 9 presents the pore size distribution of the substrate culture block. The measured pore sizes range from 500 to 14500 μm, with a concentration of pores falling within the range of 1000~6000 μm. By comparing the area covered by the pores with the total image area, it can be determined that the porosity of the substrate culture block within the same plane ranges from 40 % to 60 %.

Fig. 10(a) displays the pore recognition results for the transverse section of the substrate culture block. Fig. 10(b) displays the pore recognition results for the radial section of the substrate culture block. Fig. 10(c) displays the pore recognition results for the oblique section of the substrate culture block. In the binary image, the black and white regions represent the binarized representation, where black represents the pores, and white represents the substrate material. The vector image illustrates the division of the block to distinguish the material contour, with black representing the pores and other colors representing the substrate material.

Table 3 presents the results of measuring relevant parameters for the substrate culture block particles and pores using image

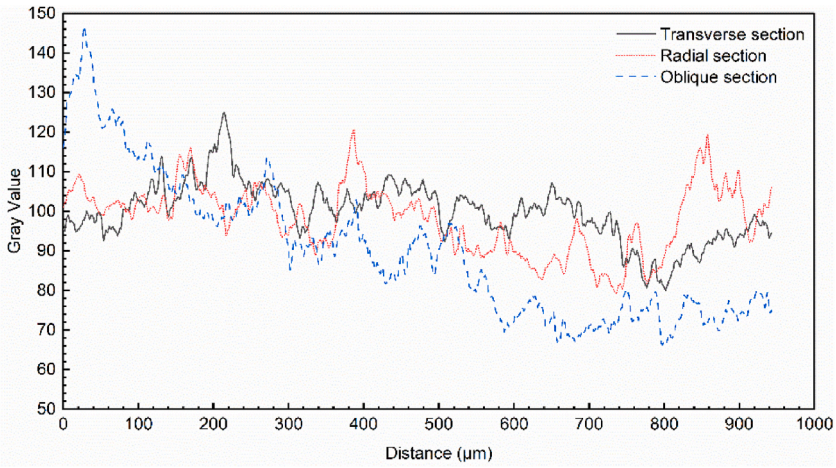

Fig. 8. Variation of gray value in different sections of substrate culture block.

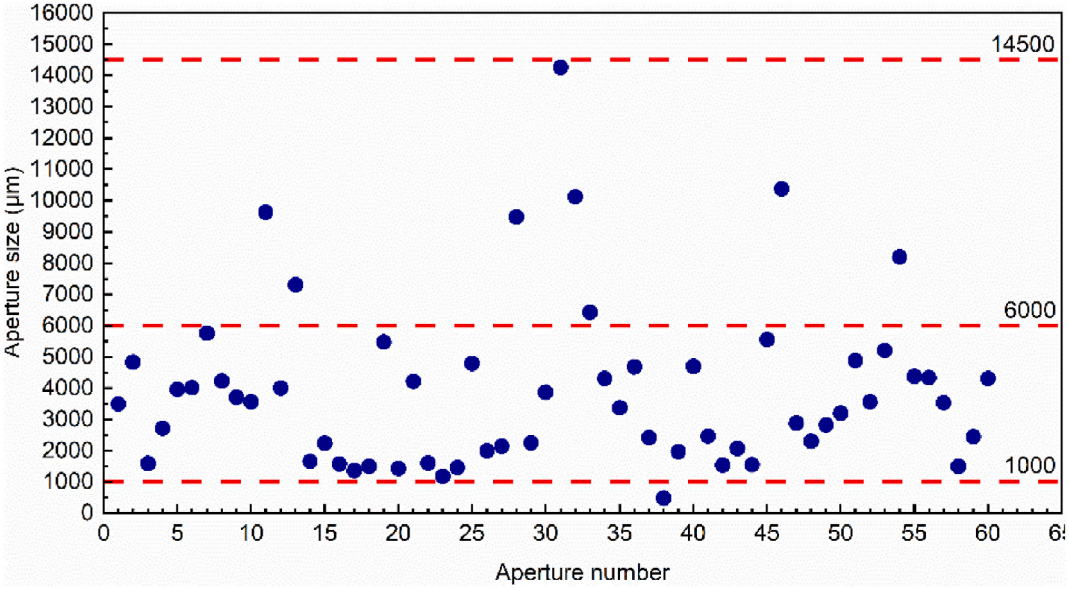

Fig. 9. Pore size distribution of substrate culture block.

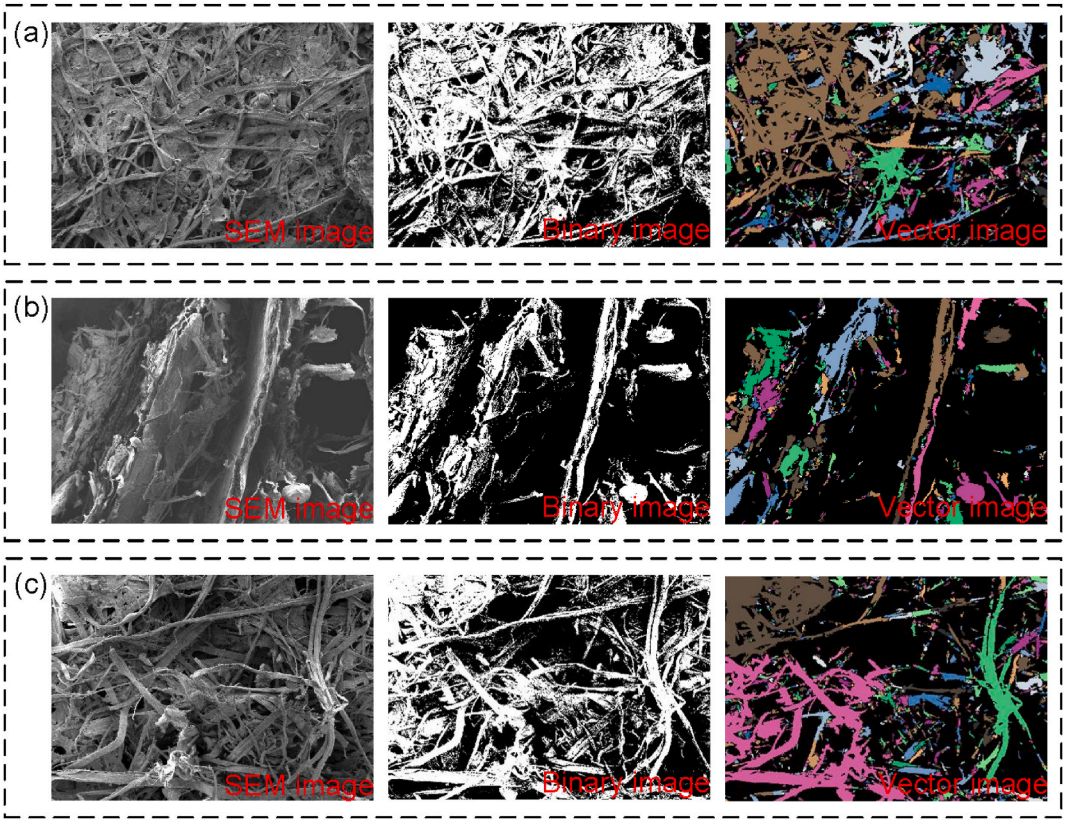

Fig. 10. Results of pore identification in three sections of the substrate culture block. (a) Transverse section, (b) Radial section, (c) Oblique section.

recognition techniques. The parameters include total pore area, average pore number, average perimeter, average number of pores, average length, average width, probability distribution index, average form factor, fractal dimension, and probability entropy. These findings are crucial for future research on the porosity of substrate culture blocks.

Table 3
Parameters related to particles and pores of substrate culture block.

Parameter	Transverse section	Radial section	Beveled section	Average
Total pore area, pixel	1144320.00	861877.00	239253.00	748483.33
Average pore area, pixel	579.38	2668.40	565.61	1271.11
Average perimeter, pixel	113.43	146.70	123.67	127.93
Pore number	884.00	323.00	423.00	543.33
Average length, pixel	29.59	33.79	34.07	32.48
Average width, pixel	15.57	18.06	15.98	16.54
Probability distribution index	1.93	1.95	1.80	1.90
Average form factor	0.36	0.39	0.35	0.37
Fractal dimension	1.26	1.18	1.25	1.23
Probability entropy	0.96	0.95	0.97	0.96

Note: Data statistics results rounded to two decimal places.

3.4. Analysis of the structural composition of pore channels

Based on the definition of porous media materials, the material properties of the substrate culture block in the initial wet base state are considered to be multiphase media. On the other hand, the material properties of the substrate culture block after drying are classified as porous media. Fig. 11(a) illustrates the substrate culture block multiphase media, which includes two types of media: solid phase media and non-solid phase media, with the non-solid phase media being further divided into liquid and gas. The shaded area in the solid phase medium indicates the solid skeleton part of the substrate culture block. In contrast, the scattered area represents the substrate culture block non-solid phase liquid, and the white area symbolizes the substrate culture block non-solid phase gas. The solid phase medium of the substrate culture block comprises straw and cow dung mixture material.

In contrast, the non-solid phase medium consists of liquid within the material and the non-solid phase gas. These three phases form a homogeneous mixed distribution, creating a unit volume block of the substrate culture block. The solid phase matrix comprises straw and cow dung mixture material that interlocks, embeds, stacks, and sticks together to form a solid skeleton. This skeleton supports the substrate cultivation body, which has a particular volume and shape, and the uniform distribution of the volume element is built into the substrate culture body's external structural performance. The solid phase matrix, straw-cow dung mixture material, liquid, gas, and other non-solid media form the pore structure throughout the substrate cultivation body. When taking an appropriate size of the volumetric element within the substrate cultivation body, the volume element contains a specific proportion of the skeleton and pore space.

Indeed, in the substrate culture block, the arrangement of material particles is irregular, leaving gaps between them. These gaps occupy space and form pores within the structure. Fig. 11(b) represents a schematic diagram of the pore structure of the substrate culture block. These pores can be categorized into channels and blind channels based on their closed state.

Channels refer to bi-directionally or multi-directionally connected pores, allowing fluid flow in multiple directions. On the other hand, blind channels represent unidirectionally closed pores, restricting fluid flow to a single direction. The channel and blind channel spaces within the substrate culture block allow the interconnectivity of non-solid phase liquid and gas throughout these regions. This means that liquids and gases in the non-solid phase media can circulate and flow within the pores.

3.5. Mechanism analysis of the internal drying process

3.5.1. Stages of drying process

The drying curve of the growing medium culture block is illustrated in Fig. 12. The temperature curve exhibits a proportional relationship with time. As time progresses, the drying temperature gradually increases before reaching a plateau. Conversely, the moisture content curve displays an inverse relationship with time. As time elapses, the moisture content steadily decreases. At

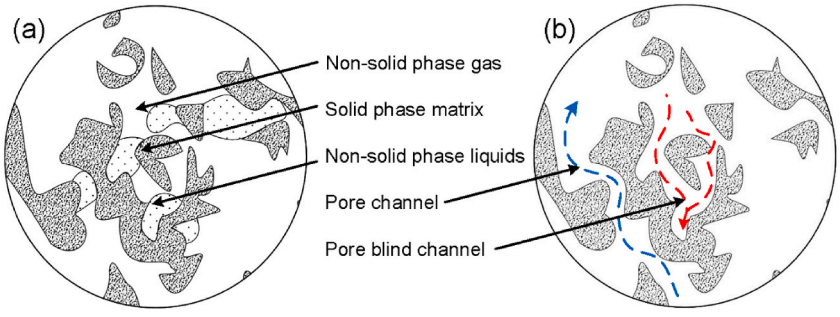

Fig. 11. Channel phase distribution and channel type of substrate culture block. (a) Multiphase media distribution of substrate culture block, (b) Pore structure of substrate culture block.

0~23min, the temperature increased from 22.9 °C to 25.6 °C. At this stage, the temperature curve intersected with the moisture content curve, and the moisture content decreased from 86.4 % to 25.6 %. The two curves intersected and then separated in the following period; with the increase in drying time, the temperature increased continuously, and the moisture content decreased continuously. 300min, the temperature increased to 39.9 °C, and the moisture content decreased to 25.2 %. Before that, the gradient of temperature and water content change was large, and then the temperature and water content had no obvious change trend, indicating that the drying of this stage was complete. Based on the variations in temperature and moisture content, the drying process can be categorized into three distinct stages: fast speed drying stage I, constant speed drying stage II, and slow speed drying stage III.

The first stage, fast speed drying stage I, is distinguished by a rising temperature and a significant reduction in water content as the non-solid phase liquid evaporates from the substrate culture block. The constant speed drying stage II is characterized by a steady temperature and a gradual decrease in water content as the substrate culture block loses non-solid phase gases. Finally, the slow speed drying stage III is marked by a gradual increase in temperature coupled with a plateauing of the water content curve, signifying the substrate culture block's loss of remaining water.

3.5.2. Process analysis of drying stages

Based on the internal moisture distribution of the substrate culture block and the identified drying process stages, the drying process commences with the initial drying stage, traverses through the fast speed drying stage, constant speed drying stage, and slow speed drying stage, and ultimately satisfies the requisite drying standards. Fig. 13 presents an illustrative depiction of the diverse stages of water conveyance within the substrate culture block drying process.

The initial drying stage, depicted in Fig. 13(a), illustrates a substrate culture block saturated with water, both internally and within the pore channels. However, there needs to be more air present within these channels. As shown in Fig. 13(b), during the fast speed drying stage, the temperature distribution in the substrate culture block becomes non-uniform due to the rapid evaporation of the water layer on the surface. Consequently, external temperatures rise while internal temperatures remain lower, leading to variations in the rate of water loss across different locations within the drying process. During this stage, the outer layer of the substrate culture block experiences rapid evaporation of free-state water, resulting in a hardening phenomenon at the intersection edges.

In Fig. 13(c), representing the constant speed drying stage, the free-state water within the pore channels of the substrate culture block begins to migrate from the interior to the exterior. This migration occurs through pore flow, as the molecular bonding force between material particles exhibits a fluctuating trend alongside the reduction in water content. At this stage, the wet base state of the skeleton prevents the collapse of the pore channels, thereby increasing the molecular bonding force. The collapse stops as the skeleton's support reaches a certain threshold, resulting in smaller pore channels and a decrease in intermolecular bonding force. Externally, the growing medium culture block manifests as a reduction in volume, a slight depression at the center, and hardened edges. Surface moisture decreases gradually from the inner circle to the outer circle.

Finally, Fig. 13(d) represents the slow drying stage, where the temperature becomes relatively consistent across each substrate culture block volumetric element. The desired moisture content is achieved, leading to hardening of the surface and edges. Water transport at this stage is minimal.

3.5.3. Forms of internal moisture existence

Fig. 14 illustrates the different forms of water present in the substrate culture block. These forms include bound-state water and free-state water. The bound-state water consists of two types: particle-attached water and capillary water. On the other hand, free-state water encompasses two types as well: surface adsorbed water and interparticle water.

Particle-attached water refers to water tightly bound to the particles of the substrate culture block. This water becomes attached to the particles through absorption and adsorption processes. It can either fill the gaps between particles or surround them, creating a wet

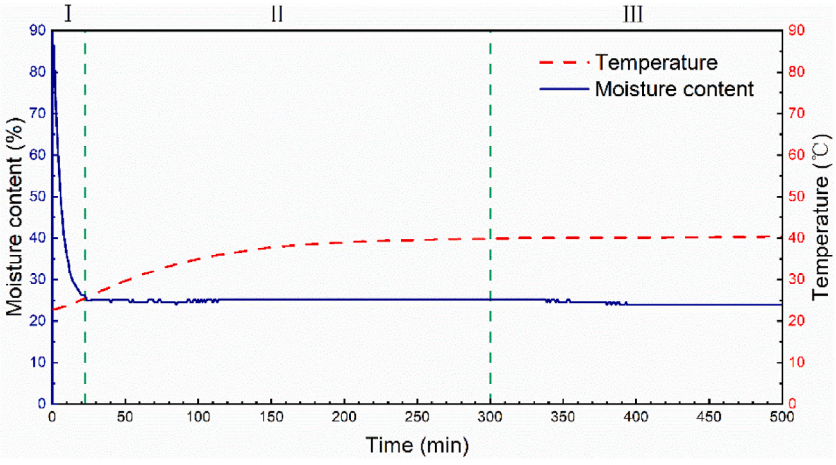

Fig. 12. Drying characteristic curve of substrate cultivator material.

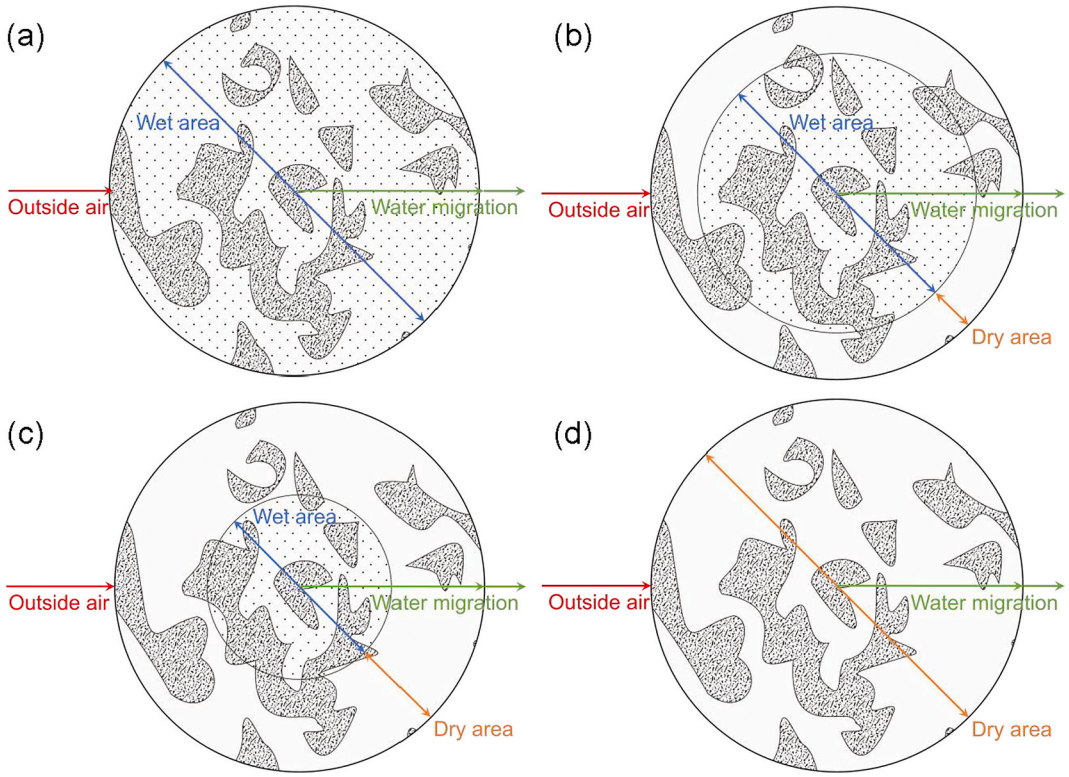

Fig. 13. Different stages of moisture migration during drying of matrix cultivars. (a) Initial drying stage, (b) Fast drying stage, (c) Constant drying stage, (d) Slow drying stage.

state for the particles. Capillary water, on the other hand, arises from capillary action within the pore spaces or capillaries between the particles. This water can transfer hydrostatic pressure and move through the capillary pore space. Most capillary water exists within a specific range of pore sizes, known as interparticle water. When the pore size is too small, the water primarily exists in a combined form. Capillary water is distributed throughout the interconnected pores within the substrate particles. These interconnected pores can be envisioned as numerous capillary tubes with various shapes and diameters.

Surface adsorbed water is free-state water that can move freely within the outer layer of the substrate culture particles. This water adheres to the surface of the particles due to the interaction between the surface and the water tension, and it becomes enveloped in the

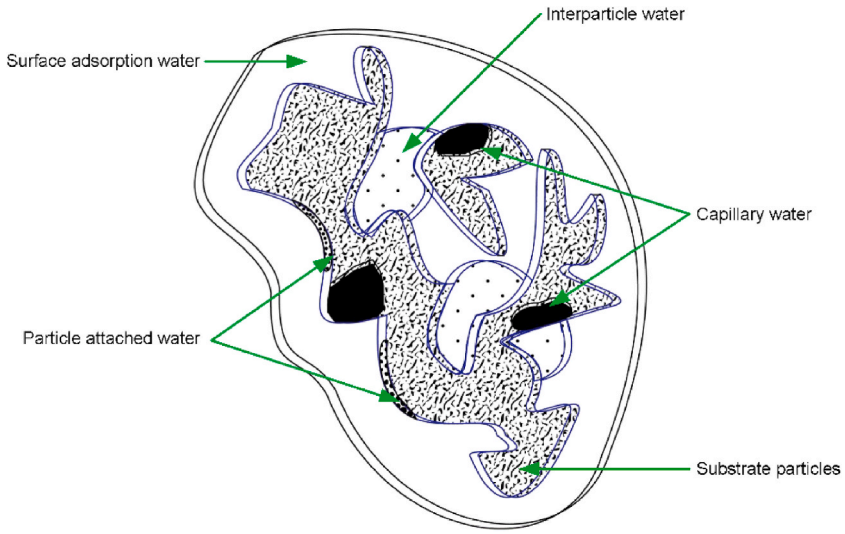

Fig. 14. Forms of water presence inside the substrate culture block.

outer layer of the material particles. Interparticle water, on the other hand, is also free-state water, but it has fewer flow constraints compared to surface-adsorbed water. This water can circulate and flow freely within the pores, moving in between the particles within the substrate culture block.

Bound-state water is crucial in forming a solid skeleton structure by combining it with the dry substrate material. When the amount of bound-state water reaches saturation, it transforms free-state water. At this point, the free-state water and air fill the pores of the substrate culture block. It can freely flow within the blind channels and channels of the pores or penetrate the skeleton structure to become bound-state water again. Free-state water evaporates During the growing medium's drying process, while bound-state water undergoes a gradient migration.

3.5.4. Internal moisture migration path

During the heat drying process of the growing medium, water in the outermost layer of the substrate evaporates first, followed by sequential transport of water from the inside to the outside. Infiltration occurs due to the priority migration of free-state water from the surface water evaporation, which moves from the inside of the pores to the outside. As the deficit of free-state water occurs, bound-state water in the substrate material evaporates. The outer layer of the substrate begins the evaporation process to create a temperature and humidity gradient, completing the wet heat exchange. Fig. 15(a–d) shows the water transport pathway for a single volumetric element, with surface-adsorbed water evaporating first, followed by interparticle water, particle-attached water, and finally, capillary water undergoing osmotic migration.

Water migration is a continuous process during drying, and it proceeds from a high gradient to a low gradient until internal and external equilibrium is achieved. Surface-adsorbed water has the largest contact area with the air and thus has priority in the water transport process. When the amount of surface-adsorbed water is less than that of other types of water, other parts of the water complete the gradient transfer, and the overall moisture content decreases, completing one cycle of the drying process.

3.6. Analysis of pore coefficient of drying process

In the pore channel modeling process shown in Fig. 16(a–d), the results display pore images during natural drying from 0 to 45 h. The points in the process are randomized to avoid biased outcomes. As the drying time increases, there is continuous loss and evaporation of water in the substrate culture block. This leads to a reduction in the volume profile of the substrate culture block. The color gradually transitions from black-brown to yellow-brown, indicating surface and internal pore structure changes.

The compactness of the substrate increases and the proportion of substrate skeleton in a unit volume of the element also increases. Consequently, the proportion of pore space decreases. In the pore image, the yellow-brown area represents the substrate skeleton, while the white area represents the pore space.

Table 4 presents the statistics of the pore coefficient ratio during the drying process, obtained through image recognition calculations. The results show that the pore coefficient ratio decreases continuously as the drying time increases, and the two variables have an inverse relationship. This confirms the reasonableness and correctness of the pore coefficient ratio.

Furthermore, the concept and calculation method of the pore coefficient ratio can be used to evaluate the drying quality of the substrate culture block and assess the effectiveness of the drying process. When the moisture content of the substrate culture block falls within the range of 20 %~30 %, the average value of the pore coefficient ratio is 40.53 %, which indicates the optimal drying time for the substrate culture block. Conversely, it can be inferred that the drying effect is best when the pore coefficient ratio of the substrate culture block is around 40 %. If the ratio deviates significantly from this level, either higher or lower, further optimization of the drying process is required.

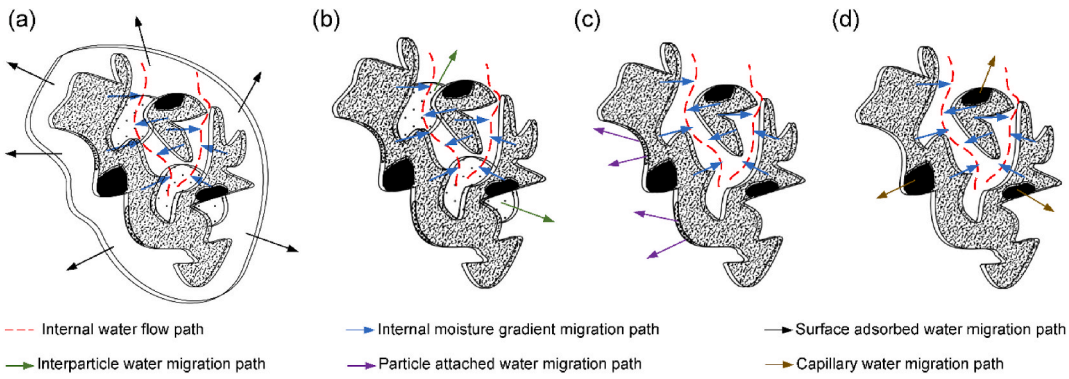

Fig. 15. Water migration pathways within the substrate culture block. (a) Surface adsorbed water migration, (b) Interparticle water migration, (c) Particle attached water migration, (d) Capillary water migration.

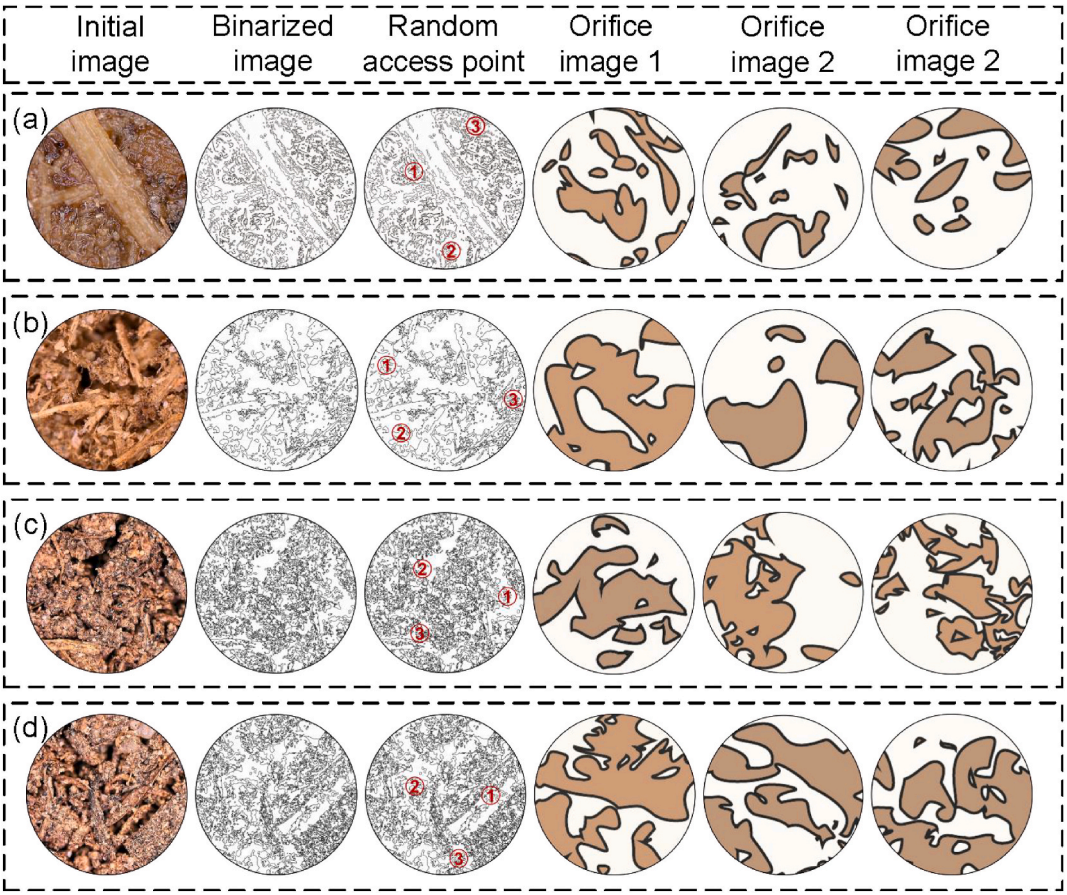

Fig. 16. Pore channel modeling process and pore channel image results under natural dry state. (a) Drying 0 h, (b) Drying 15 h, (c) Drying 30 h, (d) Drying 45 h.

Table 4
Statistics of pore coefficient ratio results for the drying process.

Drying time, h	Water content, %	Pore coefficient ratio 1	Pore coefficient ratio 2	Pore coefficient ratio 3	Average value
0	75~80	72.55	88.52	77.43	79.50
15	60~70	64.39	66.35	67.55	66.10
30	40~50	60.13	60.84	58.96	59.98
45	20~30	32.03	47.24	42.30	40.53

3.7. Statistical analysis of drying test results

In the drying test of the substrate culture block, the initial moisture content in the wet base state was 80 %, and the mass was 5068.49 g. The block was dried at a constant temperature of 60 °C for 78 h in an electric blast drying oven until a steady state was reached, and the moisture content in the dry base state was 20 %, with a mass of 2967.6 g. Fig. 17(a and b) illustrates the change in temperature and humidity during the drying process.

The temperature and humidity monitoring during the drying process of the substrate culture block revealed distinct stages of drying.

In the initial 0~10 h, the internal center temperature of the block increased from 22.9 °C to 41.9 °C, while the center humidity decreased from 66.3 % to 27.6 %. The temperature at the internal edge rose from 22.9 °C to 40.7 °C, with the edge humidity decreasing from 66.3 % to 22.6 %. This indicates a gradient difference between the center and edge in terms of temperature and humidity, suggesting incomplete drying at this stage.

During the 10~40 h, the internal center temperature further increased from 41.9 °C to 55.4 °C, accompanied by a decrease in center humidity from 27.6 % to 22.6 %. The edge temperature increased from 40.7 °C to 48 °C, while the edge humidity maintained at 22.6 %–17.5 %. The gradient difference in temperature and humidity between the center and edge was less pronounced, indicating that drying was approaching completion.

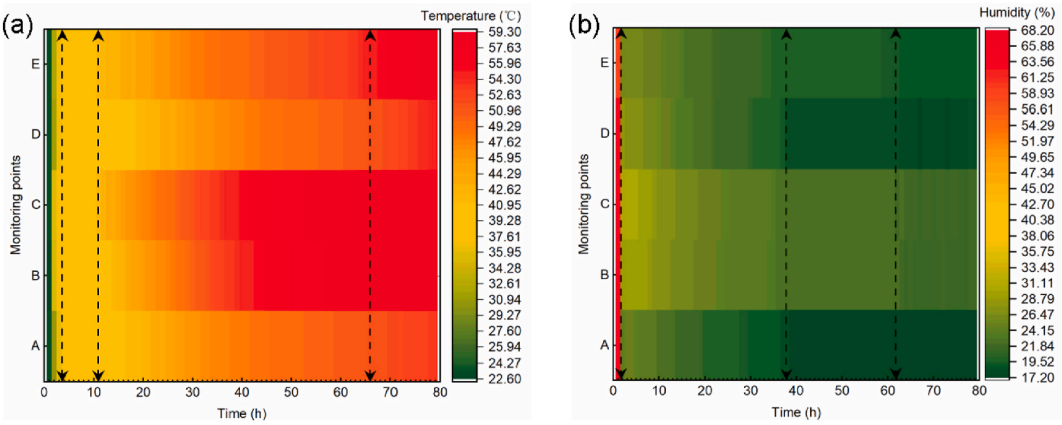

Fig. 17. Variation of temperature and humidity in drying test of substrate culture block. (a) Temperature, (b) Humidity.

From 40∼60 h, the center temperature inside the substrate culture block continued to rise slightly from 55.4 °C to 58.2 °C, while the edge temperature increased from 48 °C to 50.7 °C. The center humidity remained at 22.6 %, and the edge humidity remained at 17.5 %. The temperature showed a slight increase, but the humidity remained stable, indicating that drying was essentially complete.

Based on the observed changes in temperature and humidity, the drying process can be divided into three stages: fast speed drying stage (0∼10 h), constant speed drying stage (10∼40 h), and slow speed drying stage (40∼60 h). These divisions verify the accuracy of the stage classification in the drying process.

4. Discussion

Constructing a pore channel model for the growing medium and introducing the pore coefficient ratio are innovative approaches to evaluating the drying quality. We can evaluate the drying condition more accurately by assessing the pore condition. With this model, we can analyze how water exists within the porous media and prioritize water transport during the drying process at a micro level. This provides valuable insights into the mechanisms involved in drying porous media. The findings and methodology developed in this research can serve as a theoretical and methodological foundation for drying porous media materials. Furthermore, it can advance research and development in mass drying processes and equipment. Overall, this study contributes significantly to understanding and improving the drying of porous media, offering references for future research and development endeavors in this field.

Regarding the study of the drying mechanism, Miloš Vasić et al. analyzed the moisture transfer during the drying process of clay bricks. The study pointed out that the mechanism of moisture movement during the drying process is quite complex. No accepted explanation at this stage can determine the exact transition between the drying mechanisms. The results of the study confirmed that the effective diffusivity can represent the overall transport characteristics of moisture [41], and the practical concept of diffusivity can be combined with the pore coefficient ratio of the drying phase in this study to make the revelation of the drying mechanism more theoretical. Compared to the research process of Wei X. et al., who performed pore-scale modeling of heat-moisture and stress-strain distributions of high-moisture porous media and then revealed the drying shrinkage mechanism, the present study used more analytical tools for pore and crack analysis, which are all able to show that combining multiple pore-related image processing methods is a favorable tool for studying the drying mechanism of porous media-like materials [42]. Libin Tan et al. performed pore-scale modeling of heat-moisture and stress-strain distributions in high-moisture porous media. They analyzed them with a self-developed pore network simulation algorithm, revealing a shrinkage drying mechanism in high-moisture media [43]. Thus, developing simulation algorithms is also essential to refining the present study.

The present study utilized random access points to evaluate the pore coefficient ratio for assessing the quality of the substrate culture block after drying. While this approach avoids the possibility of biased results, it still relies on the artificial selection of the points, which may not accurately represent the entire sample. Developing a program or software for randomly accessing and identifying pores in images is necessary to achieve more accurate experimental results. Furthermore, the pore channel model constructed in this study is a two-dimensional ideal model that only exists in a single moment of static processing and analysis. However, the water transport process in substrate culture blocks is continuous and complex, adhering to fundamental laws. To further advance the understanding of the drying mechanism in porous media-like materials, it is essential to construct a three-dimensional pore channel model that penetrates the substrate culture block and analyzes it thoroughly, combining the two models to improve the theory and viewpoints stated in this study continuously.

5. Conclusions

(1) The physicochemical properties of the growing medium were measured, and the results were compared with the industry standards, which showed that the physicochemical properties of the substrate culture block were within a reasonable range and could provide the required nutrient environment for plant growth.
(2) A scanning electron microscope was used to characterize the transverse section, radial section, and oblique section of the substrate culture block, and the results showed that there were abundant pore structures and pore channels inside the substrate culture block, which provided abundant water holding sites and water transport channels during the drying process.
(3) The pore and particle conditions of the substrate culture block were measured and analyzed. The pore structure was rich, and the pores were uniformly distributed in all directions. The pore size distribution ranged from 500 to 14500 μm, the pore size was concentrated in 1000∼6000 μm, and the porosity of the substrate culture block in the same plane was between 40 % and 60 %.
(4) The pore channel model of the substrate culture block was constructed according to the Table structure of the substrate culture block and the structural characteristics of the porous medium, which revealed that the distribution of the multi-phase medium of the substrate culture block at the microscopic level was that the solid phase medium was the backbone to play a supporting role, and the non-solid phase gases and liquids were uniformly filled in the backbone.
(5) According to the measurement of the drying rate, the drying stages of the substrate culture block were divided into fast speed drying stage, constant speed drying stage, and slow drying stage. The form of water existence in the growing medium is differentiated into bound-state water and free-state water. The priority of water transport was surface-adsorbed water, inter-particle water, particle-attached water, and capillary water.
(6) The pore channel model was constructed by defining the pore coefficient ratio and recording the sample morphology of different drying stages of substrate culture block at 0∼45 h of drying. The pore coefficient ratio was calculated for the samples of different stages of substrate culture block; the average value of the pore coefficient ratio after 10 h of drying was 79.50 %, and the average value of the pore coefficient ratio after 45 h of drying was 40.53 %, at this time, the moisture content of the growing medium is 20 %∼30 %, which meets the drying requirements. At this time, the water content of the substrate cultivar was 20 % ∼30 %, which was in line with the drying requirements. The pore coefficient ratio quantitatively analyzes the reasonableness and correctness of the change situation of the pore channel in the drying process.
(7) According to the results of the drying test of the substrate culture block, the correctness of the drying stage division was verified. After drying at a constant temperature of 60 °C for 78 h, the temperature and humidity of the substrate culture block reached a steady state. The moisture content of the dry substrate state was 20 %, and the mass was 2967.6 g.

Data availability statement

All data generated or analyzed during this study are included in this published article.

CRediT authorship contribution statement

Qian Cheng: Writing – review & editing, Writing – original draft, Visualization, Investigation, Formal analysis. **Zihui Liu:** Validation, Software. **Jiayi Sun:** Visualization, Data curation. **Shuo Li:** Visualization, Software. **Chongxuan Zhao:** Project administration, Data curation. **Junfeng Su:** Validation, Investigation, Data curation. **Qingyu Liu:** Methodology, Conceptualization. **Mingjin Xin:** Supervision, Resources. **Dejun Liu:** Writing – review & editing, Validation, Resources, Methodology, Conceptualization.

Declaration of competing interest

The authors declare that they have no known competing financial interests or personal relationships that could have appeared to influence the work reported in this paper.

Acknowledgements

The authors would acknowledge the financial support provided by Boruiwei (Liaoning) Electromechanical Technology Co., Ltd.

References

[1] B. Chen, S. Mohrmann, H.T. Li, M. Gaff, R. Lorenzo, I. Corbi, O. Corbi, K.D. Fang, M. Li, Research and application progress of straw, J. Renew. Mater. 11 (2) (2023) 599–623. https://10.32604/jrm.2022.022452.
[2] D.X. Li, Y.L. Wang, D.J. Lu, X.Q. Chen, Z.L. Cui, X.P. Chen, J.W. Lu, J. Nie, H.Y. Wang, J.M. Zhou, Bio-straw resource recycling systems: agricultural productivity and green development, Resour. Conserv. Recycl. 190 (2023) 106844. https://10.1016/j.resconrec.2022.106844.
[3] J.H. Yin, D.J. Li, J.Y. Yu, X. Bai, W.J. Cui, R. Liu, M.H. Zhuang, Environmental and economic benefits of substituting chemical potassium fertilizer with crop straw residues in China, Environ. Sci. Pollut. Res. 30 (11) (2023) 30603–30611. https://10.1007/s11356-022-24128-9.
[4] H.J. Yin, W.Q. Zhao, T. Li, X.Y. Cheng, Q. Liu, Balancing straw returning and chemical fertilizers in China: role of straw nutrient resources, Renew. Sust. Energ. Rev. 81 (2018) 2695–2702. https://10.1016/j.rser.2017.06.076.
[5] A. Satlewal, R. Agrawal, S. Bhagia, P. Das, A.J. Ragauskas, Rice straw as a feedstock for biofuels: availability, recalcitrance, and chemical properties, Biofuels Bioprod. Biorefining 12 (1) (2018) 83–107. https://10.1002/bbb.1818.

[6] S.N. Harun, M.M. Hanafiah, N.M. Noor, Rice straw utilisation for bioenergy production: a brief overview, Energies 15 (15) (2022) 5542. https://10.3390/en15155542.

[7] R. Zhang, X. Li, J.G. Fadel, Oyster mushroom cultivation with rice and wheat straw, Bioresour. Technol. 82 (3) (2002) 277–284. https://10.1016/s0960-8524(01)00188-2.

[8] N. Wu, F.H. Tian, O. Moodley, B. Song, C.W. Jia, J.Q. Ye, R.N. Lv, Z. Qin, C.T. Li, Optimization of agro-residues as substrates for pleurotus pulmonarius production, Amb. Express 9 (1) (2019) 184. https://10.1186/s13568-019-0907-1.

[9] C. Sarnklong, J.W. Cone, W. Pellikaan, W.H. Hendriks, Utilization of rice straw and different treatments to improve its feed value for ruminants: a review, Asian Australas, J. Anim. Sci. 23 (5) (2010) 680–692. https://10.5713/ajas.2010.80619.

[10] B. Shrivastava, K.K. Jain, A. Kalra, R.C. Kuhad, Bioprocessing of wheat straw into nutritionally rich and digested cattle feed, Sci. Rep. 4 (2014) 6360. https://10.1038/srep06360.

[11] X.P. Ye, J. Julson, M. Kuo, A. Womac, D. Myers, Properties of medium density fiberboards made from renewable biomass, Bioresour. Technol. 98 (5) (2007) 1077–1084. https://10.1016/j.biortech.2006.04.022.

[12] J.T. Aladejana, Z.Z. Wu, M.Z. Fan, Y.Q. Xie, Key advances in development of straw fibre bio-composite boards: an overview, Mater. Res. Express 7 (1) (2020) 012005. https://10.1088/2053-1591/ab66ec.

[13] Q.F. Zhang, R.Y. Wang, W.W. Liu, Y.C. Yang, L.L. Huang, E.R. Huo, Z. Ma, New strategy for reinforcing polylactic acid composites: towards the insight into the effect of biochar microspheres, Int. J. Biol. Macromol. 245 (2023) 125487. https://10.1016/j.ijbiomac.2023.125487.

[14] K. Sharma, V.K. Garg, Comparative analysis of vermicompost quality produced from rice straw and paper waste employing earthworm eisenia fetida (Sav.), Bioresour. Technol. 250 (2018) 708–715. https://10.1016/j.biortech.2017.11.101.

[15] R. Sharda, A. Singh, K. Pandey, Paddy and maize straw-based media as an alternative for cocopeat in soilless cultivation, J. Plant Nutr. 46 (20) (2023) 4679–4697. https://10.1080/01904167.2023.2240848.

[16] H.X. Wang, J.L. Xu, L.X. Sheng, H.W. Teng, Study on treatment of city tail water by constructed wetland with corn straw biochar substrate, Environ. Technol. Innov. 28 (2022) 102855. https://10.1016/j.eti.2022.102855.

[17] K. Shukla, R. Mishra, P. Sarkar, Understanding soilless engineered soil as a sustainable growing material for food production in a green roof, Mater. Today Proc., Manipal University Jaipur, Rajasthan, INDIA 43 (5) (2021) 3054–3060. https://10.1016/j.matpr.2021.01.397.

[18] A. Graceson, M. Hare, N. Hall, J. Monaghan, Use of inorganic substrates and composted green waste in growing media for green roofs, Biosyst. Eng. 124 (2014) 1–7. https://10.1016/j.biosystemseng.2014.05.007.

[19] M.G. Jahromi, A. Aboutalebi, Garden compost as a substrate for vegetable transplant production, Acta Hortic. 898 (2011) 165–170. https://10.17660/ActaHortic.2011.898.19.

[20] M. Xin, T. Chen, Q. Zhang, J. Jiao, X. Bai, Y. Song, R. Zhao, C. Wei, Parameters optimization for molding of vegetable seedling substrate nursery block with rice straw, Nongye Gongcheng Xuebao 33 (16) (2017) 219–225. https://10.11975/j.issn.1002-6819.2017.16.029.

[21] L. Dejun, Z. Yanji, L. Kun, C. Qian, B. Xuewei, G. Yuanjuan, Experimental study on molding technology for making seedling block based on maize stovers, Nongye Gongcheng Xuebao 36 (5) (2020) 241–248. https://10.11975/j.issn.1002-6819.2020.05.028.

[22] L. Dejun, W. Jiaxin, Z. Yanj, L. Tianqi, L. Yuge, S. Jiayi, L. Zihui, Forming mechanism and experiment of greening substrate bricks pressed by using agricultural organic waste, Nongye Gongcheng Xuebao 38 (12) (2022) 243–252. https://10.11975/j.issn.1002-6819.2022.12.028.

[23] T.Q. Liu, J.X. Wang, Y.G. Li, Z.H. Liu, J.Y. Sun, D.J. Liu, Design and experiment of substrate grass seed blanket extrusion device, Sustainability 14 (17) (2022) 11046. https://10.3390/su141711046.

[24] K.D. Nona, B. Lenaerts, E. Kayacan, W. Saeys, Bulk compression characteristics of straw and hay, Biosyst. Eng. 118 (2014) 194–202. https://10.1016/j.biosystemseng.2013.12.005.

[25] L. Ma, L. Sha, X.X. Liu, S.T. Zhang, Study of molding and drying characteristics of compressed municipal sludge-corn stalk fuel pellets, Energies 14 (11) (2021) 3116. https://10.3390/en14113116.

[26] R.L. Li, H.Y. Wang, E.Z. Duan, J.Y. Fan, L.J. Wang, Rabbit manure compost for seedling nursery blocks: suitability and optimization of the manufacturing production process, Agriculture-Basel 12 (12) (2022) 2156. https://10.3390/agriculture12122156.

[27] J.J. Fu, Z.C. Cui, Y.S. Chen, C.S. Guan, M.J. Chen, B. Ma, Simulation and experiment of compression molding behavior of substate block suitable for mechanical transplanting based on discrete element method (DEM), Agriculture-Basel 13 (4) (2023) 883. https://10.3390/agriculture13040883.

[28] J. Zheng, X. Shi, J. Shi, Z. Chen, Pore structure reconstruction and moisture migraton in porous media, Fractals-Complex Geom, Patterns Scaling Nat. Soc. 22 (3) (2014) 1440007. https://10.1142/s0218348x14400076.

[29] X.H. Tan, L. Jiang, X.P. Li, Y.Y. Li, K. Zhang, A complex model for the permeability and porosity of porous media, Chem. Eng. Sci. 172 (2017) 230–238. https://10.1016/j.ces.2017.06.041.

[30] S.Y. Suo, L.S. Jiang, P. Wang, M.Z. Xie, Study of the porous media random structure model, Mod. Phys. Lett. B 34 (10) (2020) 2050090. https://10.1142/s0217984920500906.

[31] V.M. Melnyk, V.D. Rud, Y.A. Melnyk, Correctness of fractal analysis of fractographic surface microstructure according to digital SEM photogrammetry, Powder Metall. Met. Ceram. 57 (5–6) (2018) 353–360. https://10.1007/s11106-018-9991-z.

[32] X. Tang, Y.M. Zhu, Y. Liu, Investigation of shale nano-pore characteristics by scanning electron microscope and low-pressure nitrogen adsorption, J. Nanosci. Nanotechnol. 17 (9) (2017) 6252–6261. https://10.1166/jnn.2017.14485.

[33] E. Keita, Particle deposition in drying porous media, Materials 14 (18) (2021) 5120. https://10.3390/ma14185120.

[34] C. Liu, B. Shi, J. Zhou, C. Tang, Quantification and characterization of microporosity by image processing, geometric measurement and statistical methods: application on SEM images of clay materials, Appl. Clay Sci. 54 (1) (2011) 97–106. https://10.1016/j.clay.2011.07.022.

[35] C. Liu, C.-S. Tang, B. Shi, W.-B. Suo, Automatic quantification of crack patterns by image processing, Comput. Geosci. 57 (2013) 77–80. https://10.1016/j.cageo.2013.04.008.

[36] E. Beckers, E. Plougonven, C. Roisin, S. Hapca, A. Leonard, A. Degre, X-ray microtomography: a porosity-based thresholding method to improve soil pore network characterization? Geoderma 219 (2014) 145–154. https://10.1016/j.geoderma.2014.01.004.

[37] C.S. Choi, Y.K. Lee, J.J. Song, Equivalent pore channel model for fluid flow in rock based on microscale x-ray ct imaging, Materials 13 (11) (2020) 2619. https://10.3390/ma13112619.

[38] Y.J. Yuan, Y.D. Yuan, Y.Y. Xu, J.X. Dong, X.D. Liu, Numerical and experimental fractal pore network study on drying of porous media: model building, Adv. Mater. Res., Guangzhou, CHINA 557–559 (2012) 2159–2162. https://10.4028/www.scientific.net/AMR.557-559.2159.

[39] Y.J. Yuan, Y.D. Yuan, Y.Y. Xu, J.X. Dong, X.D. Liu, Numerical and experimental fractal pore network study on drying of porous media: numerical simulation, Adv. Mater. Res., Guangzhou, CHINA 557–559 (2012) 2167–2170. https://10.4028/www.scientific.net/AMR.557-559.2167.

[40] Y.J. Yuan, Z. Zhao, J.N. Nie, Y.Y. Xu, Pore network analysis of zone model for porous media drying, Math. Probl Eng. 2014 (2014) 624145. https://10.1155/2014/624145.

[41] M. Vasic, Z. Grbavcic, Z. Radojevic, Analysis of moisture transfer during the drying of clay tiles with particular reference to an estimation of the time-dependent effective diffusivity, Dry. Technol. 32 (7) (2014) 829–840. https://10.1080/07373937.2013.870194.

[42] X. Wei, K.V. Bicalho, A. El Hajjar, S. Taibi, M. Hattab, J.M. Fleureau, Experimental techniques for the study of the cracking mechanisms in drying clays, Geotech. Test J. 44 (2) (2021) 323–338. https://10.1520/gtj20190430.

[43] L.B. Tan, Y.J. Yuan, Z. Zhao, Y.Y. Xu, Y.D. Yuan, Insights in mechanism of drying shrinkage by pore-scale modeling of heat-moisture and stress-strain distribution for high-moisture porous media, Int. J. Therm. Sci. 188 (2023) 108226. https://10.1016/j.ijthermalsci.2023.108226.